Proceedings in Applied Mathematics and Mechanics

SPECIAL ISSUE 95th Annual Meeting of the International Association of Applied Mathematics and Mechanics (GAMM)

RESEARCH ARTICLE OPEN ACCESS

Quasivoids in Polydisperse Glassy Systems With Atomistic PEL Exploration and Iso-Configuration Method

Guan-Qiang Liu[1] | S. Swayamjyoti[2] | Normand Mousseau[3] | Man-Kin Fung[4] | Cho-Tung Yip[1] | Bernd Markert[2] | Franz Bamer[2]

[1]School of Science, Harbin Institute of Technology (Shenzhen), Shenzhen, China | [2]Institute of General Mechanics, RWTH Aachen University, Aachen, Germany | [3]Department of Physics and Institut Courtois, Université de Montréal, Montréal (QC), Canada | [4]School of Science and Technology, Hong Kong Metropolitan University, Hong Kong, China

Correspondence: S. Swayamjyoti (swayamjyoti@iam.rwth-aachen.de)

Received: 18 August 2025 | **Revised:** 7 April 2026 | **Accepted:** 13 April 2026

Keywords: activation–relaxation technique (ARTn) nouveau | polydisperse glasses | quasivoids

ABSTRACT

Understanding the microscopic relaxation mechanisms in amorphous solids remains a fundamental challenge. A theoretical framework posits that dynamics are mediated by quasivoids: transient, localized quasi-particles that are the amorphous analogue of crystalline vacancies. Unlike a simple void, a quasivoid consists of fragmented, distributed free volume that is collectively reassembled to accommodate an atomic hop. In this work, we investigate these elementary relaxation events by exploring the potential energy landscape (PEL) of a model polydisperse glass using the activation–relaxation technique nouveau (ARTn), an open-ended algorithm designed to efficiently locate transition saddle points on the PEL. By analyzing 4910 independent activated events, we find that structural relaxations are highly localized, typically involving a small number of atoms (1–6), and are characterized by energy barriers uncorrelated with the net energy change of the event. Visualization of the atomic trajectories reveals that these events manifest as string-like cooperative motions. Crucially, we provide a direct, atom-resolved visualization of a relaxation cascade where the presence of a quasivoid facilitates an initial atomic hop, which in turn effectively transports the quasivoid, enabling subsequent hops along the chain. These results offer computational evidence for the role of quasivoids as fundamental defect-like excitations that trigger string-like structural relaxations, providing a physical basis for dynamics in amorphous materials.

1 | Introduction

1.1 | Quasivoid

When a fluid undergoes rapid cooling, its atoms or molecules cannot rearrange quickly enough to form an ordered crystalline structure, resulting in a disordered amorphous state—that is, a glass. The viscosity of glass increases significantly (often by several orders of magnitude). Although glass is often referred to as a supercooled liquid, it exhibits all the mechanical properties of a solid. However, the nature of the phase transition from liquid to glass remains an unresolved problem in physics.

In crystalline materials, vacancy defects serve as the primary carriers for atomic diffusion, with their positions directly identifiable by the absence of atoms. However, the disordered structure of glasses has long posed challenges for both the definition and observation of vacancies. The free volume theory initially postulated that "voidlike" regions drive particle motion [1], but subsequent experiments revealed only weak correlations between

local density and dynamics [2], along with the inability to precisely define free volume boundaries at the molecular scale [3]. In 2020, Berthier et al. noted: "The fundamental discrepancy between free volume theory and the kinetic constraint model (KCM) lies in the absence of microscopically observable defect entities" [4].

String-like cooperative motion has been identified as a fundamental form of dynamical heterogeneity in glass-forming liquids, a phenomenon originally characterized by Donati et al. [5]. The theoretical connection between these dynamical strings and thermodynamic concepts, such as configurational entropy within the Adam–Gibbs framework, was subsequently established by Starr et al. [6]. A recent comprehensive review by Xu et al. [7] further highlights the universality of string-like motion as the microscopic realization of cooperative rearranging regions (CRR) across various disordered systems. To address the structural origin of these dynamics, Zhang and Lam, building upon the kinetic constraint model framework [8], proposed the distinguishable particle lattice model (DPLM) [9], which for the first time quantitatively linked vacancy defects to string-like motion. The model posits that voids propagate kinetic excitations by inducing string-like motion; the heterogeneous potential energy distribution of particles leads to fractal characteristics in void migration pathways. The DPLM not only successfully reproduces the dynamic features of fragile glasses [10] but also resolves the Kovacs expansion gap paradox [10], establishing a new paradigm for defect-driven theories. Further advancing this framework, Lam introduced the configuration tree theory [11], which abstracts the evolution of system configurations into a tree-like network. By employing mean-field approximation, the theory analytically computes relaxation times that show excellent agreement with simulation results.

Colloidal systems, serving as "scaled-up atomic glasses," provide a unique platform for validating theoretical models. In 2015, Nagamanasa et al. observed through two-dimensional colloidal experiments that particle motion at high densities was predominantly characterized by collective cluster modes, with string-like motion significantly diminished [12]. This finding raised questions about the universality of dynamic facilitation theory. To address this discrepancy, Yip and colleagues introduced a temporal-scale decomposition method. Through ultralong-duration observations ($> 10^6$ s), the apparent cluster motion was demonstrated to actually represent superimposed segments of string-like motion. More critically, through tracking the endpoints of string-like motion, they identified "quasivoids"—transient free-volume regions generated by collective particle displacements. These quasivoids exhibit memory effects in their migration pathways: in glass/crystal interface experiments, upon entering the crystalline phase, quasivoids transform into conventional vacancy defects, diffuse through the lattice, and subsequently return to the glassy matrix to initiate new cycles of string-like motion [13]. This discovery not only provides a physical embodiment for the free volume concept but also reveals a coupled mechanism governing glass–crystal interfacial dynamics.

1.2 | Inherent Structure and the Activation–Relaxation Technique nouveau

In 1969, Goldstein proposed the concept of the potential energy landscape (PEL) to understand the properties of supercooled liquids [14]. He suggested that at low temperatures, glassy systems predominantly evolve near local minima of the PEL. These local minima, termed inherent structures, represent energy-minimized configurations of the glass. These local minima are separated by energy barriers significantly exceeding the thermal energy. Consequently, the dynamics of glassy systems can be conceptualized as transitions between potential energy basins within the PEL. In real space, these dynamics manifest as particle hopping events, corresponding to transitions between local minima in the PEL. Subsequently, inherent structures have been extensively studied as their dynamics provide crucial insights into microscopic relaxation processes in glasses. Notably, these potential energy minima represent local minima of the total potential energy of the system. The short-time β-relaxation corresponds to the system's evolution within a single potential energy basin. While temperature reduction does not significantly affect intra-basin evolution, it substantially hinders inter-basin transitions, thereby requiring longer relaxation times. In contrast to short-time, localized relaxation processes, the long-time α-relaxation represents the system's evolution across multiple inherent structures over extended periods. Over the past three decades, numerous numerical methods have been developed for sampling the PEL of complex materials. Most approaches focus on transition state searches and energy barrier calculations, many of which require prior knowledge of both initial and final states of the system. However, in complex systems where known states are limited, researchers have increasingly favored open-ended algorithms under such circumstances. The activation–relaxation technique nouveau (ARTn) represents one such open-ended algorithm for locating first-order saddle points [15–17]. Since its initial proposal in 1996, ARTn has undergone more than two decades of refinement and development. By incorporating the Lanczos algorithm while combining features of eigenvector-following methods and dimer approaches, it achieves precise identification of first-order saddle points. The algorithm explores the PEL by converging from a local potential energy minimum to adjacent saddle points. Through ARTn, we can drive the system's evolution between different inherent structures, enabling direct investigation of relaxation mechanisms and energy landscape dynamics in disordered materials.

The ARTn has emerged as a powerful method for investigating the atomistic PEL of disordered solids by efficiently identifying saddle points and connected local minima far beyond the reach of traditional molecular dynamics. Traditional molecular dynamics is limited by the time-scale problem, where it cannot capture long time-scale processes with required efficiency. In a comprehensive review of molecular mechanics in disordered solids, the methodology's capacity for exploring complex atomistic potential energy landscapes (PEL) in amorphous materials—including those with inherent structural heterogeneity—-was underscored [18]. Complementing this, a study on model two-dimensional network glasses elucidated the atomistic origins of

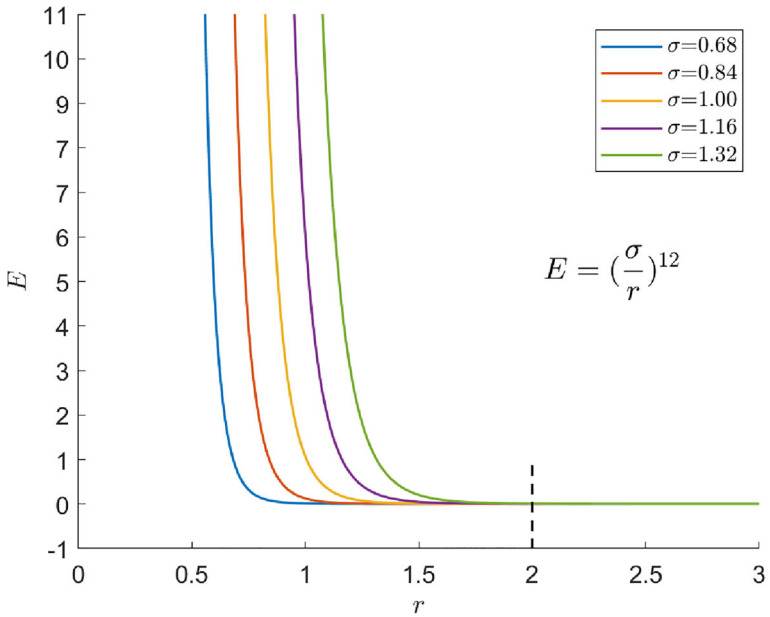

FIGURE 1 | The interaction potential between identical atoms as a function of distance, where the black dashed line indicates the truncation position.

reversible and irreversible atomic rearrangements, showcasing how ARTn can distinguish between local, reversible relaxations, and permanent structural modifications [19]. Extending this line of research, a relevant investigation of a model 2D Zachariasen silica glass under shear and pressure resolved understanding of elementary plastic events and clarified how shear-driven and pressure-assisted processes mediate the transition from microscopic reversible to macroscopic irreversible responses [20].

2 | Sample Preparation

We employed the Lennard–Jones potential for our samples but retained only the repulsive term. This purely repulsive potential accelerates simulation time without sacrificing physical realism and has been successfully applied in previous studies [21, 22, 23]. To simulate a polydisperse system, we introduced 128 distinct atom types in our samples.

Thus, the potential function we used is

$$V_{ij} = \begin{cases} \varepsilon\left(\frac{\sigma_{ij}}{r}\right)^n, & r < r_c \\ 0, & r \geq r_c \end{cases} \tag{1}$$

where σ_{ij} is determined by the non-additive mixing rule

$$\sigma_{ij} = \frac{\sigma_i + \sigma_j}{2}\left(1 - \varepsilon_0|\sigma_i - \sigma_j|\right). \tag{2}$$

The potential energy versus distance profiles for different σ_{ij} values are shown in Figure 1. We introduced a non-additivity parameter $\epsilon_0 = 0.2$, which promotes proximity between particles with large size differences, thereby suppressing fractionation within the system. This combination of size polydispersity and nonadditivity has been shown to produce highly stable glass formers [24, 25]. All quantities in our simulations are expressed in Lennard–Jones (LJ) units. The unit of length is the mean particle diameter $\bar{\sigma}$, and we take $\bar{\sigma} = 1$. The individual particle diameters, σ_i, are drawn from a uniform distribution ranging from 0.68 to 1.32. The parameter ϵ defines the unit of energy. Consequently, the unit of time becomes $\bar{\sigma}\sqrt{m/\epsilon}$, where $m = 1$ is the mass of each particle. By setting the Boltzmann constant $k_B = 1$, the unit of temperature also becomes ϵ. In our simulations, we also take $\epsilon = 1$, leading to dimensionless units adopted in this work. The cutoff distance r_c for interactions is uniformly set to 2. Beyond this distance, interactions are truncated, and the choice of a relatively large cutoff ensures the continuity of the potential function's derivative during the minimization phase of the ARTn event search. The total number of atoms in our simulation is 4096, meaning there are 32 atoms of each atomic type.

3 | ARTn Parameter Settings

Subsequently, the ARTn was applied to the samples. ARTn first employs the FIRE algorithm (fast inertial relaxation engine) [26] to relax the system to an initial local potential energy minimum. Upon completion of this step, ARTn proceeds to search for nearby saddle points. This is achieved by randomly selecting a central atom and displacing it and its near-neighbors within a radius of R_n from its equilibrium position by 0.05 along a random direction, thereby destabilizing the system. Here we set $R_n = 0.5$ in order to guarantee the localized nature of the perturbation. As the system is pushed iteratively away from the local minimum along this initial direction, a small perpendicular relaxation is performed to avoid collisions. At each step, the lowest eigenvalue of the corresponding Hessian matrix is determined. When this value becomes negative (we use an eigenvalue threshold of $-1.0\epsilon/\bar{\sigma}$), the system is considered having left the local harmonic basin surrounding the minimum and it is pushed along this direction of negative curvature, with a relaxation in the perpendicular

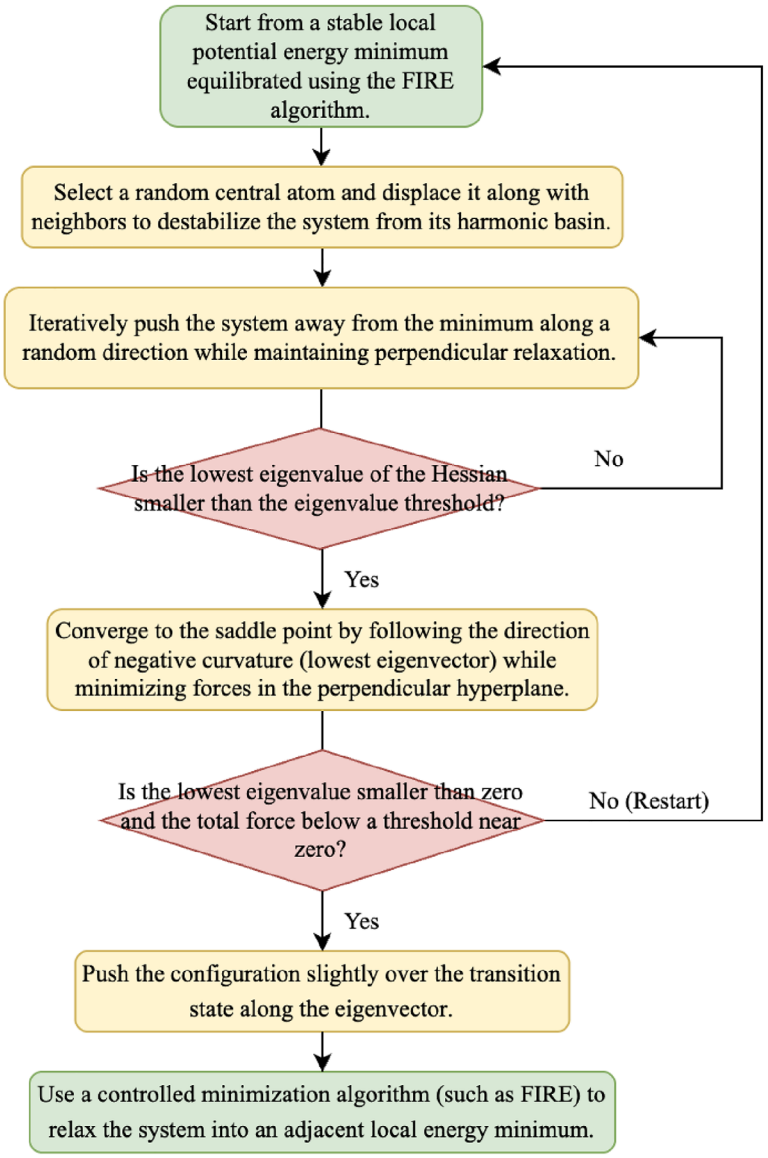

FIGURE 2 | Schematic representation of ARTn algorithm.

hyperplane, until the system's forces approach zero, at which point the system is considered to have reached a saddle point. In this step, since the initial atomic displacement direction is randomly chosen, rare cases may occur where the atom moves into an overlapping position with another atom, causing divergence in the results. Such instances were excluded from our analysis. Once the system reaches a saddle point, ARTn reactivates the FIRE algorithm to relax the system from the saddle point to a new potential energy minimum, with an additional FIRE minimization step, which ensures that it is possible to go back to the initial minimum from the saddle point and, hence, that the pathway is reversible. This process—from the initial minimum energy configuration to a saddle point and then to another minimum energy configuration—constitutes a single ARTn event. A schematic flowchart summarizing this algorithmic workflow, including the activation, convergence, and relaxation phases, is presented in Figure 2. After completing an ARTn event, the system was restored to its initial configuration, and ARTn was restarted to obtain new events. To ensure statistical reliability, we collected 4910 valid events for subsequent analysis. We note that the identified structural relaxations are highly localized, typically involving fewer than 10 atoms (as detailed in Section 5). Consequently, our system of 4096 particles is effectively large enough to avoid boundary interference with these local events.

4 | Protocol for Obtaining Initial Configuration

We employed the Metropolis algorithm within ARTn to iteratively relax the system energy and obtain a sufficiently low-energy configuration. If the potential energy of the relaxed configuration was lower than that of the initial configuration, the new configuration was accepted with probability 1. Otherwise, the new configuration was accepted with probability $\exp(-\Delta E/k_B T)$. Here, the temperature was treated as a virtual parameter, which was set to $k_B T = 0.1$, a value chosen to facilitate the escape from shallow local minima while ensuring convergence toward

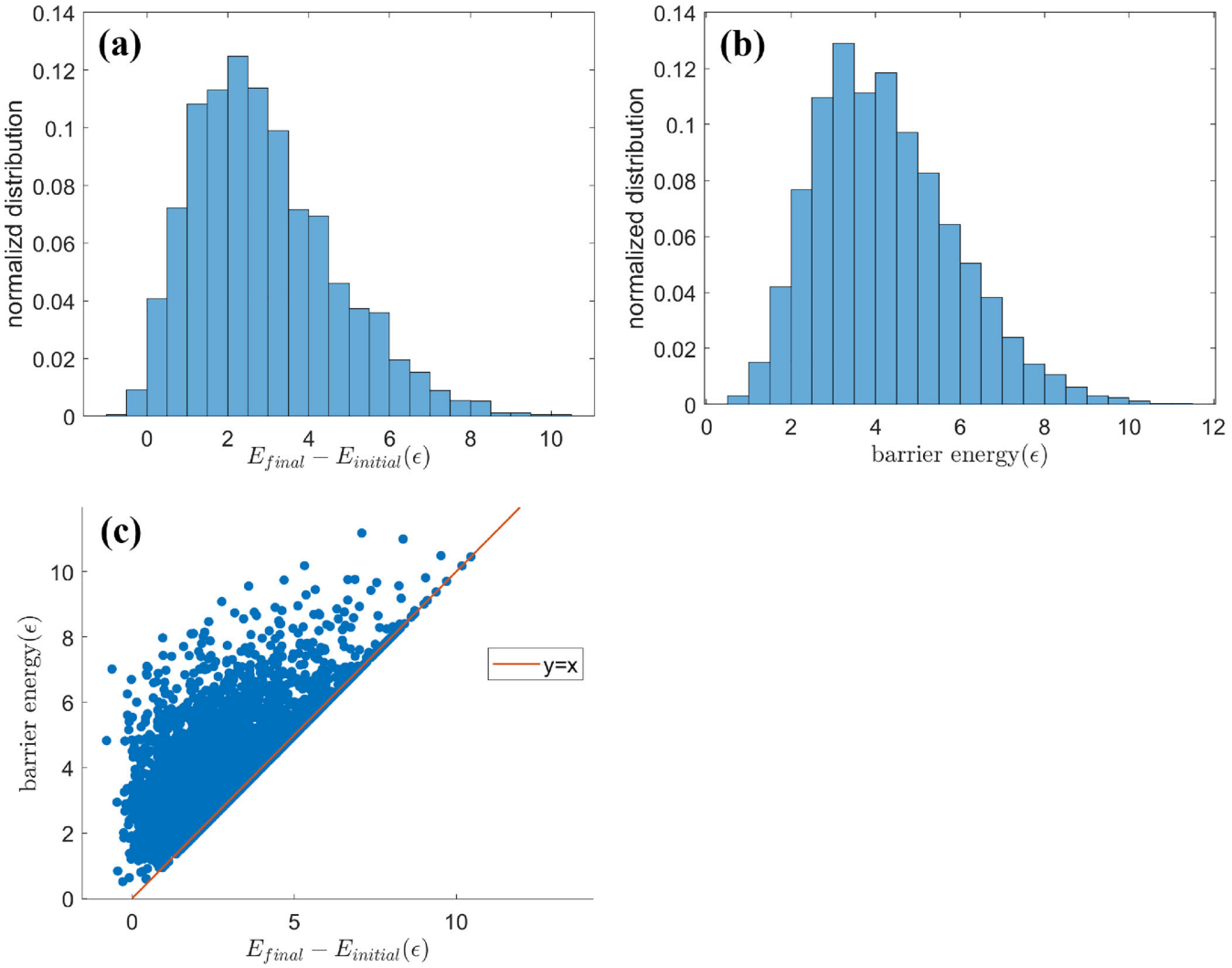

FIGURE 3 | (a) Normalized distribution of the change in energy between the initial and final state configurations. (b) Normalized distribution of barrier energies. (c) a scatter plot of this energy difference with the corresponding barrier energy.

low-energy inherent structures. The Metropolis procedure was terminated when no energy reduction was observed over 500 consecutive events, indicating that the system had reached a sufficiently low-energy state. Starting from such low-energy configurations for saddle-point searches enabled the acquisition of more stable system configurations and ensured that nearly all events were localized.

5 | Results

Starting from the stable initial configurations of our system, statistical analysis of the collected 4910 events yielded the distribution of energy differences between initial and final states, as shown in Figure 3a. The results demonstrate that in the vast majority of cases, the system's energy increased after an event, with only 1% of exceptions. This confirms that our initial configurations resided at sufficiently low energies, suggesting they were located at the bottom of a deep basin in the energy landscape [27]. Figure 3b presents the normalized distribution of energy barriers, defined as the difference between saddle-point energy and initial energy. The barrier energy peaks around 3ϵ, with the distribution approaching zero when barrier energies become sufficiently small. The very few negative-energy barriers are associated with narrow unstable deformations that remain in the system, even after minimization. Figure 3c displays a scatter plot correlating the energy changes between initial and final atomic configurations with their corresponding barrier energies. As observed in other systems [27], except for the fact that the system's energy barrier cannot be smaller than the energy difference between initial and final states, there is no correlation between the barrier energy and the energy difference.

To quantify atomic participation in each activation–relaxation event, we calculated the participation number (PN) [28] using the established methodology from Ref. [29]. The PN is defined as

$$\omega_i = \frac{|\Delta\vec{R}_i|^4}{\sum_{i=1}^{N} |\Delta\vec{R}_i|^4} \tag{3}$$

$$PN = \frac{1}{\sum_{i=1}^{N} \omega_i^2}. \tag{4}$$

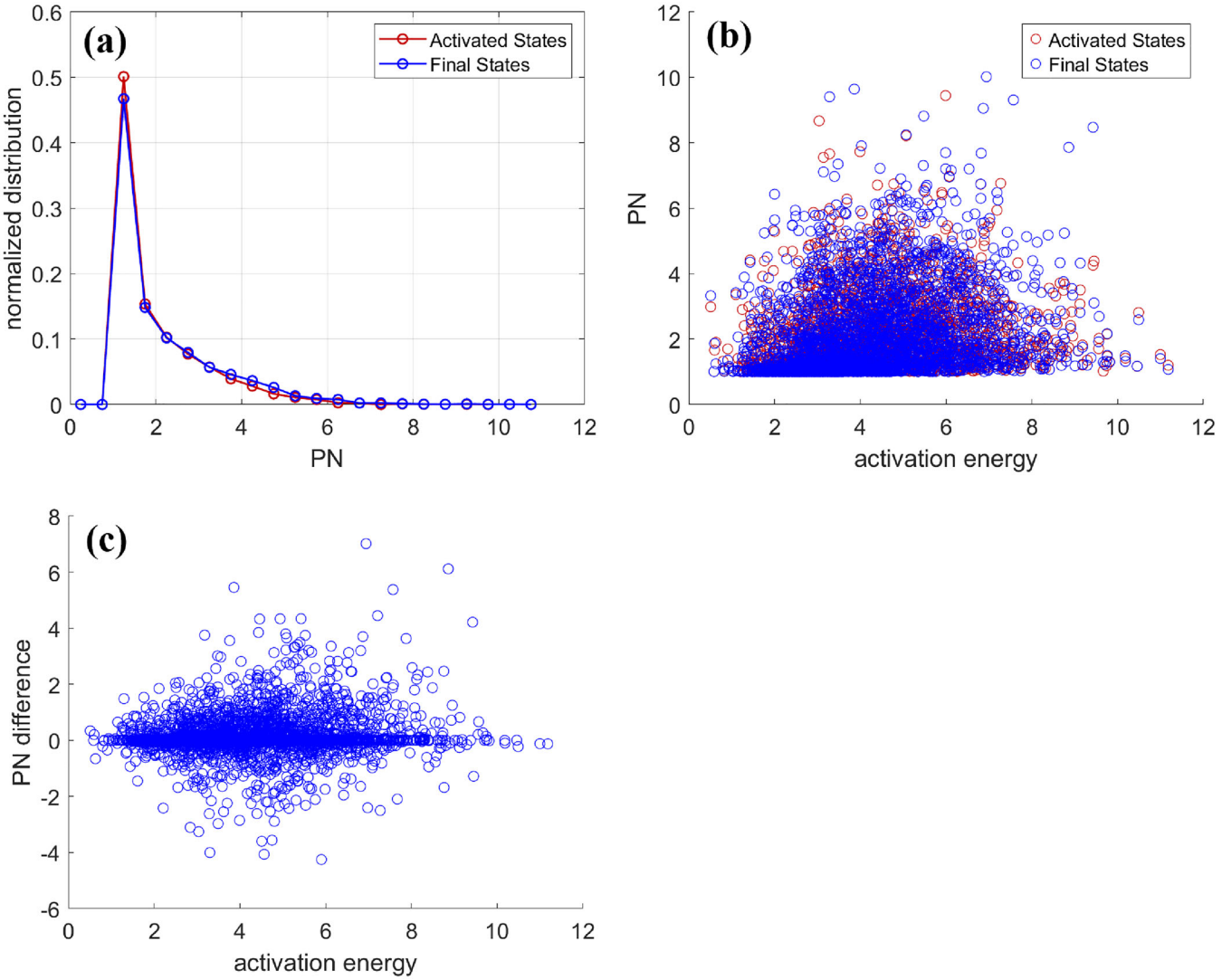

FIGURE 4 | (a) Histogram of participation number (b) Scatter plot of participation number (PN) of activated and final state configurations against activation energy (c) scatter plot of participation-number difference between the connected activated and final states as a function of activation energy.

Here N denotes the total number of atoms. The PN varies between 1 and N. When only one atom moves, PN equals 1, meaning the moving atom carries a weight of 1 while all others have zero weight. When the weight is evenly distributed among all atoms in the system, PN reaches N. In this scenario, all atoms in the sample displace by identical distances, demonstrating equal participation in the process.

Figure 4a presents the distribution of PN values, revealing that most events typically involve 1 to about 6 atoms, with approximately 60% events involving 3 atoms or less. No significant difference exists between the PN values of activation and relaxation processes, indicating no strong bias toward having more or fewer participating atoms in the final state compared to the activated state. Interestingly, as shown in Figure 4b, the number of participating atoms does not grow with the energy barriers, but is maximal in the middle of the energy-barrier distribution: events possessing either the lowest or highest barrier energies involve only a few atoms. Figure 4c displays the difference in participation numbers between activation and relaxation processes, demonstrating that the participation number may decrease or increase by several atoms; this is compatible with previous observations in amorphous silicon that the forward barrier and the reverse barrier (from connecting the final minimum to the saddle point) are uncorrelated [27]. These mechanisms are of the same nature, however, and, on average, the variation in participation number approaches zero, consistent with the results shown in Figure 4a.

5.1 | Visualization

Next, we visualized some of the events identified by ARTn. Figure 5 illustrates the typical characteristics of these events. In all examples, the initial and final positions of atoms are represented by green and orange spheres, respectively. Red arrows indicate displacement from the initial to the activated position, while blue arrows represent displacement from the activated to the final position. Only atoms with a displacement greater than 0.2 are shown, whether between the initial and activated configurations or between the activated and final configurations. The atom IDs are labeled numerically to the right of their

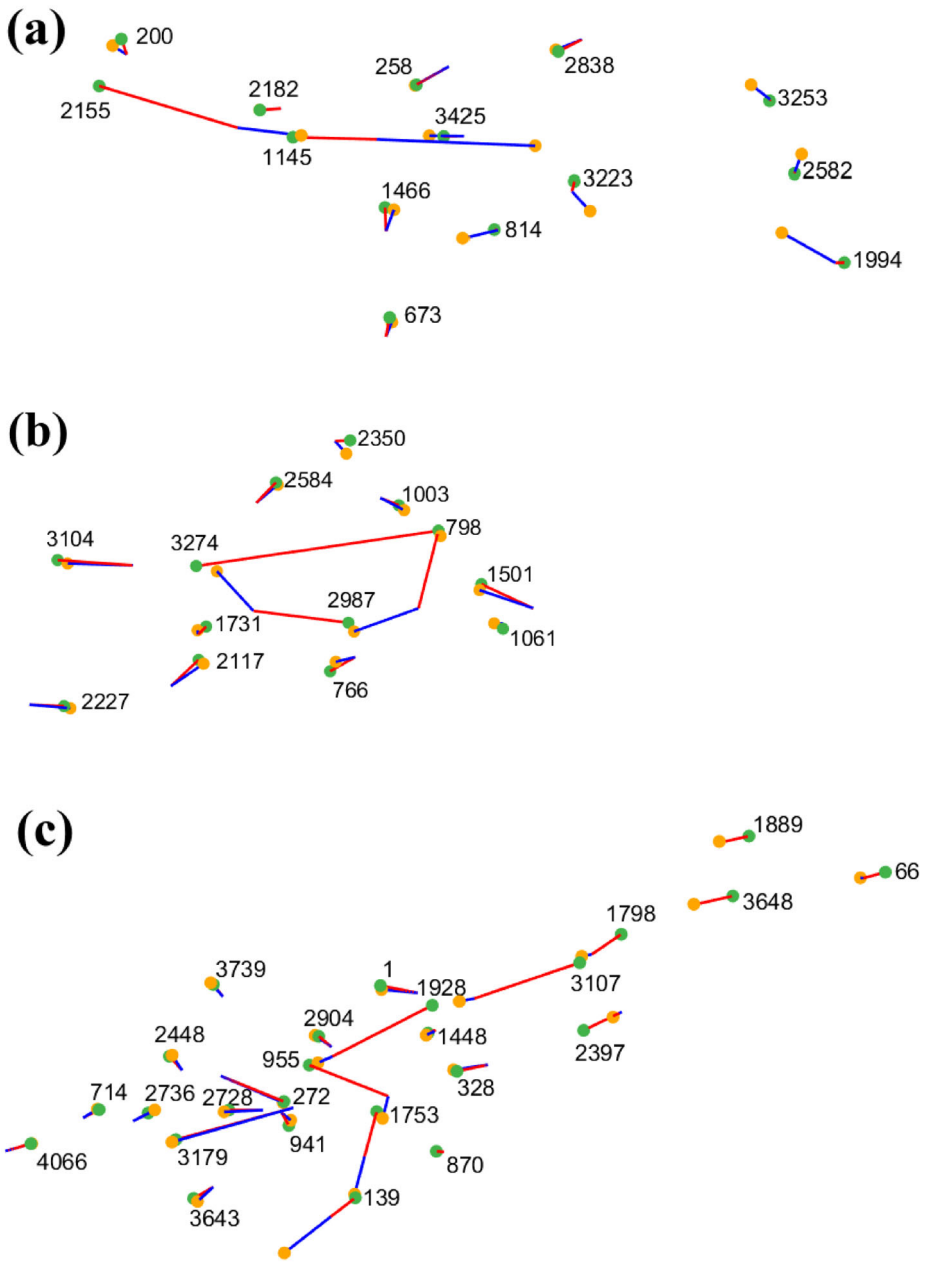

FIGURE 5 | Three examples of events identified by ARTn are displayed. In each instance, initial atomic positions are visualized with green spheres, and final atomic positions with orange spheres. Atomic displacements from the initial to the activated state are represented by red arrows, while blue arrows indicate displacements from the activated to the final state.

positions. In these examples, we consistently observed string-like motion. Figure 5a depicts a localized event involving 14 atoms with an energy barrier of 4.67 ϵ. Only three atoms, specifically those with IDs 2155 and 1145, are shown to participate in string-like motion. Most surrounding atoms oscillate around their original positions, indicating their involvement in the surrounding elastic accommodation. Figure 5b shows a localized event with an energy barrier of 3.14 ϵ, involving 13 atoms. The string-like motion formed by the central atoms creates a closed loop, while the surrounding atoms remain oscillating around their original positions. This exemplifies an elastic accommodation mechanism around an inner-loop plastic rearrangement. Figure 5c presents a localized event with an energy barrier of 9.08 ϵ, involving 25 atoms. The number of atoms participating in string-like motion is significantly higher than in the previous two examples. Consistent with the earlier examples, the surrounding atoms are involved in either elastic or plastic accommodation.

5.2 | Quasivoid-Excited String-Like Motion

The string-like motion of particles can be interpreted as the transport of quasivoids within the system. Unlike a conventional vacancy in crystalline lattices, a quasivoid in disordered glassy systems does not exist as a single, well-defined empty site. Instead, it manifests as a localized region of fragmented free volume distributed among neighboring particles. This local

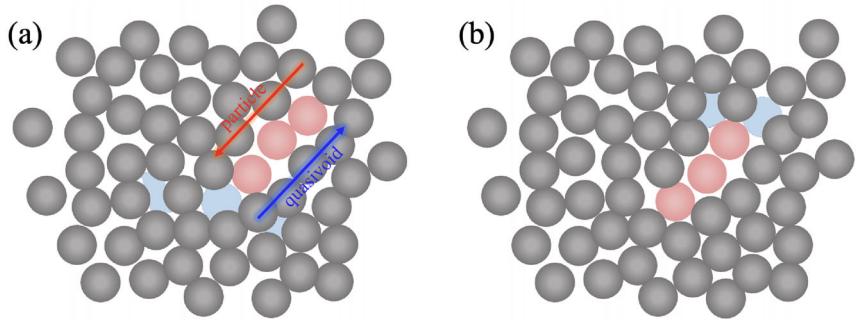

FIGURE 6 | Schematic illustration of string-like motion mediated by a quasivoid. The red spheres highlight atoms participating in the cooperative string-like motion, while the blue regions indicate the quasivoid. Comparison between the (a) initial and (b) final states demonstrates how the atomic hopping sequence effectively transports the quasivoid structure in the direction opposite to the atomic flow.

structural looseness acts as an excitation center, lowering the energy barrier for rearrangement. To clarify this mechanism, a schematic representation of the quasivoid migration process is provided in Figure 6. As illustrated in the initial state Figure 6a, the quasivoid is identified as a region of fragmented free volume (highlighted in blue), which acts as the trigger for the cooperative rearrangement. This excitation induces a string-like motion, represented by the chain of red atoms. Upon completion of the event Figure 6b, the collective hopping of these atoms fills the initial free volume, effectively transporting the quasivoid to the other end of the string. This demonstrates the retrograde migration of the quasivoid relative to the atomic flow. In our simulation results, Figure 7a is a reconstruction of Figure 5a. Due to the presence of quasivoids in Region 2, particle 1145 is able to move into Region 2, subsequently transferring the quasivoids to the particles' initial positions. The presence of the quasivoids at particle 1145's initial position then further facilitates the movement of particle 2155 to particle 1145's initial position, thereby transferring the quasivoids to Region 1. Figure 7b–d depicts events occurring after Figure 7a. These configurations are obtained by setting the system's initial configuration to the final configuration of Figure 7a and designating particle 2155 as the initially randomly moving particle. Therefore, in Figure 7b–d, the initial position of particle 2155 corresponds to its final position in Figure 7a. It is observed that the movement of particle 2155 in Figure 7b–d consistently results in string-like motion, which is attributed to the presence of quasivoids near particle 2155. Notably, in Figure 7d, particle 2155 hops back to its initial position as shown in Figure 7a. From an energy landscape perspective, the green atoms in Figure 7a correspond to configuration A in the energy landscape, while the orange atoms correspond to configuration B. In contrast, the green atoms in Figure 7b–d all represent the same configuration B, and the orange atoms represent different final configurations, denoted as C. These two string-like motions facilitate a transition of the system among three metastable states, specifically from A to B to C. Furthermore, the energy barriers that the system needs to overcome for each hop are not consistent.

6 | Iso-Configuration Method

Our research employs an iso-configuration method similar to those described in references [21, 22]. We constructed iso-configurational ensembles using the following methodology.

Initially, an equilibrated glass system was selected as the starting configuration. This system comprised 4096 particles, with their initial positions denoted as $r_i(0)$. We then simulated M independent iso-configurational ensembles, $r_i(0), v_i^m(0)$, where $m = 1, 2, \ldots, M$; $v_i^m(0)$ represents the velocity of particle i in the mth iso-configuration.

Figure 8 provides a schematic illustration of the iso-configuration ensemble structure. Based on the instantaneous particle position vector $r_i(t)$, we investigated the displacement of each particle over time, $\Delta r_i = |r_i(t) - r_i(0)|$. To fully capture the particle trajectories, a coarse-grained position definition was employed: $r_i(t) = \langle r_i(t') \rangle$, where $t' \in [t, t + \Delta t]$ and $\langle \Delta r_i \rangle$ denotes the average position of particle i within the time window $[t, t + \Delta t]$. If a particle's displacement Δr_i exceeds a predefined threshold (e.g., $\sigma_{\text{hop}} = 0.6$ [30] or $\sigma_{\text{hop}} = 0.8$ [13]), the particle is determined to have undergone a hop. These hopping particles often exhibit linear arrangements, forming string-like motions. The specific threshold value should be adjusted according to the characteristics of the system under investigation.

To quantify the hopping rate ω_i for each particle, we can compute the frequency of hopping events n_i across the M iso-configurational ensembles. Within a given time interval, we can count the number of particles whose displacement exceeded the threshold (σ_{hop}). Applying transition state theory (TST), which relates a particle's hopping rate in a specific direction to its activation energy ΔE_i, we use the expression

$$\omega_i = A_i \exp\left(-\frac{\Delta E_i}{k_B T}\right) \tag{5}$$

Here, A_i represents the attempt frequency, k_B is the Boltzmann constant, and T is the system temperature. This approach allows us to calculate the energy barriers, which will then be compared with results obtained from the ARTn method.

Conclusions and Future Work

ART has been applied on polydisperse glasses and we find that the activation energy distribution and the atomic structure of the local structural excitations (LSE) are similar to that in model metallic glasses [29, 31]. Quasivoids in polydisperse glass systems can be investigated within the PEL paradigm, where

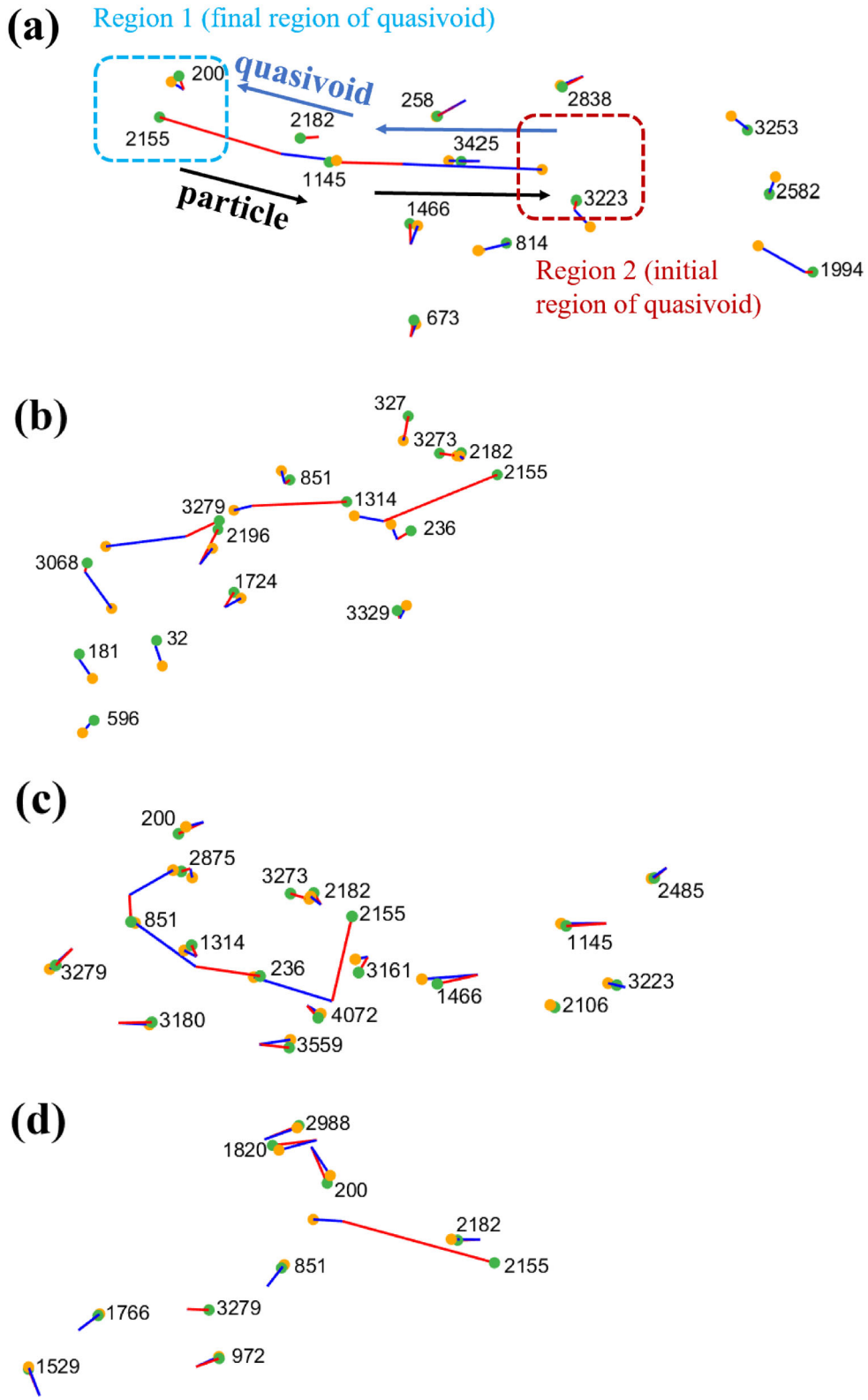

FIGURE 7 | The dynamics of quasivoids and particle movement is displayed. (a) Particles 1145 and 2155 exhibit forward hopping due to the presence of qusivoids, ultimately leading to the transfer of the quasivoids from Region 2 to Region 1. (b), (c), and (d) depict three distinct and independent events that occurred subsequent to the event shown in (a). In all figures, green atoms mark the initial positions of the particles, while orange atoms indicate their final positions. Atomic displacements from the initial to the activated state are represented by red arrows, while blue arrows indicate displacements from the activated to the final state.

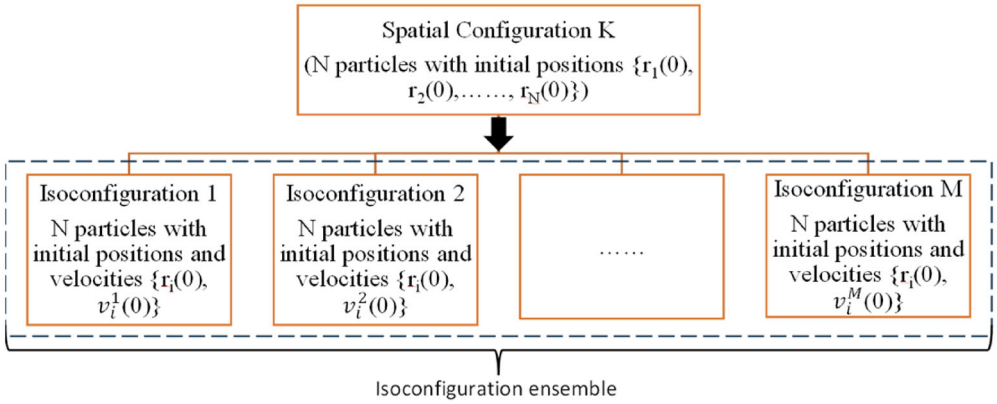

FIGURE 8 | A schematic representation of the iso-configuration method's arrangement and organizational structure is provided. In the studied system, M iso-configurational samples can be generated based on a spatial configuration K.

localized structural excitations (LSE) [29, 31] act as propagators of relaxation and plasticity; our atomistic PEL exploration technique directly investigate such LSE mechanics at zero loading conditions to locate and track quasivoid motifs across iso-configuration ensembles. To map subtle mesoscale organization around these motifs, we will in the future leverage unsupervised community-detection techniques and spectral-eigenvector tools tailored for spatial particle networks [32, 33], while supervised surrogates and feature learning from the materials and machine learning community will influence interpretation and screening of glassy materials [34, 35].

Acknowledgments

The authors thank Prof. C.H. Lam at Hong Kong Polytechnic University for valuable ideas and scientific interactions with G.Q.L. and S.S.

Open access funding enabled and organized by Projekt DEAL.

Funding

S.S., B.M., and F.B. thank Deutsche Forschungsgemeinschaft (DFG) - grant / project number 523939420 for funding.

Conflicts Of Interest

The authors do not have any conflict of interest.

Data Availability Statement

Can be provided upon request to swayamjyoti@iam.rwth-aachen.de.

References

1. D. Turnbull and M. H. Cohen, "Free-Volume Model of the Amorphous Phase: Glass Transition," *Journal of Chemical Physics* 34, no. 1 (1961) 120–125, https://doi.org/10.1063/1.1731549.

2. J. C. Conrad, F. W. Starr, and E. R. Weeks, "Weak Correlations Between Local Density and Dynamics Near the Glass Transition," *Journal of Physical Chemistry B* 109, no. 44 (2005): 21235–21240, https://doi.org/10.1021/jp0514168.

3. F. Arceri, F. P. Landes, L. Berthier, et al., "Glasses and Aging: A Statistical Mechanics Perspective," in *Encyclopedia of Complexity and Systems Science* (Springer, 2022), https://doi.org/10.1007/978-3-642-27737-5_248-2.

4. L. Berthier, G. Biroli, J. P. Bouchaud, et al., "Theoretical Perspective on the Glass Transition and Amorphous Materials," *Reviews of Modern Physics* 93 (2021): 041001, https://doi.org/10.1103/RevModPhys.93.041001.

5. C. Donati, J. F. Douglas, W. Kob, S. J. Plimpton, P. H. Poole, and S. C. Glotzer, "Stringlike Cooperative Motion in a Supercooled Liquid," *Physical Review Letters* 80 (1998) 2338–2341, https://link.aps.org/doi/10.1103/PhysRevLett.80.2338.

6. F. W. Starr, J. F. Douglas, and S. Sastry, "The Relationship of Dynamical Heterogeneity to the Adam-Gibbs and Random First-Order Transition Theories of Glass Formation," *Journal of Chemical Physics* 138, no. 12 (02 2013): 12A541, https://doi.org/10.1063/1.4790138.

7. W.-S. Xu, J. F. Douglas, and Z.-Y. Sun, "Polymer Glass Formation: Role of Activation Free Energy, Configurational Entropy, and Collective Motion," *Macromolecules* 54, no. 7 (2021) 3001–3033, https://doi.org/10.1021/acs.macromol.0c02740.

8. G. H. Fredrickson and H. C. Andersen, "Kinetic Ising Model of the Glass Transition," *Physical Review Letters* 53 (1984): 1244, https://doi.org/10.1103/PhysRevLett.53.1244.

9. L.-H. Zhang and C.-H. Lam, "Emergent Facilitation Behavior in a Distinguishable-Particle Lattice Model of Glass," *Physical Review B* 95 (2017): 184202, https://doi.org/10.1103/PhysRevB.95.184202.

10. M. Lulli, C. S. Lee, H. Y. Deng, C. T. Yip, and C. H. Lam, "Spatial Heterogeneities in Structural Temperature Cause Kovacs Expansion Gap Paradox in Aging of Glasses," *Physical Review Letters* 124 (2020): 095501, https://doi.org/10.1103/PhysRevLett.124.095501.

11. C.-H. Lam, "Local Random Configuration-Tree Theory for String Repetition and Facilitated Dynamics of Glass," *Journal of Statistical Mechanics* 2018 (2018): 023301, https://doi.org/10.1088/1742-5468/aaac56.

12. K. H. Nagamanasa, S. Gokhale, A. K. Sood, et al., "Direct Measurements of Growing Amorphous Order and Non-Monotonic Dynamic Correlations in a Colloidal Glass-Former," *Nature Physics* 11 (2015): 403–408, https://doi.org/10.1038/nphys3289.

13. C.-T. Yip, D. L. Cheung, G. Wang, et al., "Direct Evidence of Void-Induced Structural Relaxations in Colloidal Glass Formers," *Physical Review Letters* 125 (2020): 258001, https://doi.org/10.1103/PhysRevLett.125.258001.

14. M. Goldstein, "Viscous Liquids and the Glass Transition: A Potential Energy Barrier Picture," *Journal of Chemical Physics* 51 (1969): 3728–3739, https://doi.org/10.1063/1.1672587.

15. G. T. Barkema and N. Mousseau, "Event-Based Relaxation of Continuous Disordered Systems," *Physical Review Letters* 77 (1996): 4358–4361, https://doi.org/10.1103/PhysRevLett.77.4358.

16. N. Mousseau and G. T. Barkema, "Traveling Through Potential Energy Landscapes of Disordered Materials: The Activation-Relaxation

Technique," *Physical Review E* 57 (1998): 2419–2424, https://doi.org/10.1103/PhysRevE.57.2419.

17. R. Malek and N. Mousseau, "Dynamics of Lennard-Jones Clusters: A Characterization of the Activation-Relaxation Technique," *Physical Review E* 62 (2000): 7723–7728, https://doi.org/10.1103/PhysRevE.62.7723.

18. F. Bamer, F. Ebrahem, B. Markert, and B. Stamm, "Molecular Mechanics of Disordered Solids," *Archives of Computational Methods in Engineering* 30, no. 3 (2023) 2105–2180, https://doi.org/10.1007/s11831-022-09861-1.

19. F. Ebrahem, F. Bamer, and B. Markert, "Origin of Reversible and Irreversible Atomic-Scale Rearrangements in a Model Two-Dimensional Network Glass," *Physical Review E* 102, no. 3 (2020): 033006, https://doi.org/10.1103/PhysRevE.102.033006.

20. F. Bamer, F. Ebrahem, and B. Markert, "Elementary Plastic Events in a Zachariasen Glass Under Shear and Pressure," *Materialia* 9 (2020): 100556, https://doi.org/10.1016/j.mtla.2019.100556.

21. A. Widmer-Cooper, P. Harrowell, and H. Fynewever, "How Reproducible are Dynamic Heterogeneities in a Supercooled Liquid?" *Physical Review Letters* 93 (2004): 135701, https://doi.org/10.1103/PhysRevLett.93.135701.

22. A. Widmer-Cooper and P. Harrowell, "Predicting the Long-Time Dynamic Heterogeneity in a Supercooled Liquid on the Basis of Short-Time Heterogeneities," *Physical Review Letters* 96 (2006): 185701, https://doi.org/10.1103/PhysRevLett.96.185701.

23. A. Widmer-Cooper, H. Perry, and P. Harrowell, "Irreversible Reorganization in a Supercooled Liquid Originates From Localized Soft Modes," *Nature Physics* 4 (2008): 711–715, https://doi.org/10.1038/nphys1025.

24. L. Berthier, P. Charbonneau, A. Ninarello, M. Ozawa, and S. Yaida, "Zero-Temperature Glass Transition in Two Dimensions," *Nature Communications* 10 (2019): 1508, https://doi.org/10.1038/s41467-019-09512-3.

25. A. Ninarello, L. Berthier, and D. Coslovich, "Models and Algorithms for the Next Generation of Glass Transition Studies," *Physical Review X* 7 (2017): 021039, https://doi.org/10.1103/PhysRevX.7.021039.

26. E. Bitzek, P. Koskinen, F. Gähler, M. Moseler, and P. Gumbsch, "Structural Relaxation Made Simple," *Physical Review Letters* 97 (2006): 170201, https://doi.org/10.1103/PhysRevLett.97.170201.

27. H. Kallel, N. Mousseau, and F. Schiettekatte, "Evolution of the Potential-Energy Surface of Amorphous Silicon," *Physical Review Letters* 105 (2010): 045503, https://doi.org/10.1103/PhysRevLett.105.045503.

28. R. J. Bell and P. Dean, "Atomic Vibrations in Vitreous Silica," *Discussions of the Faraday Society* 50 (1970): 55–61, https://doi.org/10.1039/DF9705000055.

29. S. Swayamjyoti, J. F. Löffler, and P. M. Derlet, "Local Structural Excitations in Model Glasses," *Physical Review B* 89 (2014): 224201, https://doi.org/10.1103/PhysRevB.89.224201.

30. C.-H. Lam, "Repetition and Pair-Interaction of String-Like Hopping Motions in Glassy Polymers," *Journal of Chemical Physics* 146 (2017): 244906, https://doi.org/10.1063/1.4990417.

31. S. Swayamjyoti, J. F. Löffler, and P. M. Derlet, "Local Structural Excitations in Model Glass Systems Under Applied Load," *Physical Review B* 93 (2016): 144202, https://doi.org/10.1103/PhysRevB.93.144202.

32. R. Kishore, S. Swayamjyoti, Z. Nussinov, and K. K. Sahu, "Performance Traits of a Newly Proposed Modularity Function for Spatial Networks: Better Assessment of Clustering for Unsupervised Learning," *IOP Conference Series: Materials Science and Engineering* 872, no. 1 (2020): 012017, https://doi.org/10.1088/1757-899X/872/1/012017.

33. R. Kishore, S. Swayamjyoti, S. Das, et al., "Visual Machine Learning: Insight Through Eigenvectors, Chladni Patterns, and Community Detection in 2D Particulate Structures," *International Journal for Multiscale Computational Engineering* 20, no. 3 (2022): 125–145, https://doi.org/10.1615/IntJMultCompEng.2022041422.

34. S. Das, H. Pegu, K. K. Sahu, et al., "Machine Learning in Materials Modeling–Fundamentals and the Opportunities in 2D Materials," in *Synthesis, Modelling and Characterization of 2D Materials and Their Heterostructures* (Elsevier, 2020), 445–468, https://doi.org/10.1016/B978-0-12-818475-2.00019-2.

35. G. R. Arumugam Kumar, K. Arora, M. Aggarwal, et al., "Structure–Property Predictions in Metallic Glasses: Insights From Data-Driven Atomistic Simulations," *Journal of Materials Research* 40 (2025): 36–68, https://doi.org/10.1557/s43578-024-01480-9.